

Article

An Investigation into Electrodeposited Co–Ni–TiO₂ Films with Improved Mechanical and Corrosion Properties

Yuxin Wang , Zengcheng Miao, Songlin Zheng, Jiahuan Chen and Zhen He 

School of Materials Science and Engineering, Jiangsu University of Science and Technology, Zhenjiang 212000, China

* Correspondence: hezhen@just.edu.cn

Abstract: This investigation proposes the use of sol-enhanced electrodeposition to create a range of Co–Ni–TiO₂ films. The addition of TiO₂ sol controls the nucleation process and the properties of the composite films by generating TiO₂ nanoparticles in situ in the electrodeposition process. The transmission electron microscopy (TEM) and zeta potential analyses revealed a relatively homogenous distribution with particle size in the range below 100 nm for the TiO₂ nanoparticles produced. Microstructure, phase composition, hardness, friction, and corrosion resistance of Co–Ni–TiO₂ films were thoroughly investigated in relation to TiO₂ sol concentration. The results show that the addition of a limited content of TiO₂ sol upgraded Co–Ni films by producing a Co–Ni–TiO₂ film with a high dispersion of TiO₂ nanoparticles. On the other hand, too much TiO₂ sol could cause agglomeration and hinder the metal deposition process, resulting in surface pores and the deterioration of film performance.

Keywords: Co–Ni; electrodeposition; nanoparticles



Citation: Wang, Y.; Miao, Z.; Zheng, S.; Chen, J.; He, Z. An Investigation into Electrodeposited Co–Ni–TiO₂ Films with Improved Mechanical and Corrosion Properties. *Coatings* **2023**, *13*, 783. <https://doi.org/10.3390/coatings13040783>

Academic Editor: JongHyeon Lee

Received: 28 February 2023

Revised: 4 April 2023

Accepted: 15 April 2023

Published: 18 April 2023



Copyright: © 2023 by the authors. Licensee MDPI, Basel, Switzerland. This article is an open access article distributed under the terms and conditions of the Creative Commons Attribution (CC BY) license (<https://creativecommons.org/licenses/by/4.0/>).

1. Introduction

Due to their excellent mechanics, wear, corrosion, and other advantages, Co–Ni alloys are frequently used in protective coatings in various industries [1–4]. The main preparation techniques for cobalt-nickel coatings include electrodeposition, physical vapor deposition, chemical vapor deposition, and plasma spraying [5–8]. Electroplating technology has been regarded as a simple and efficient technique for preparing Co–Ni films [9,10]. The performance of a Co–Ni film cannot further satisfy the demands in some challenging service conditions, and it is of great scientific significance to further strengthen the Co–Ni film. Current methods for improving the performance of Co–Ni alloys include heat treatment, the pulse electrodeposition process, and composite electrodeposition technology [11–13]. Composite electrodeposition technology, one of the industry’s most widely employed reinforcement methods, can significantly enhance the Co–Ni alloy’s comprehensive properties [14,15].

Nanoparticles such as SiC [16], ZrO₂ [17], TN [18], WC [19], TiO₂ [20–22], and Al₂O₃ [23] have recently been utilized as the second reinforcing phase for composite electrodeposition. In traditional composite electrodeposition techniques, nanometer-sized inert particles are added to the electrolytes to create films. For instance, recent research by Rasooli et al. explored the influence of Cr₂O₃ nanoparticles on the Ni–Co–Cr₂O₃ coatings’ microstructure, mechanical properties, and corrosion-related properties, and found the incorporation of Cr₂O₃ nanoparticles could increase the nucleation amount of Co and improve the coating’s performance [24]. In another report, by examining the SiC-doped Ni–Co coating, Bakhit et al. stated that embedding SiC nanoparticles improved the Ni–Co film’s compactness and corrosion resistance [25].

However, nanoparticles with a high specific surface region and surface energy can easily result in agglomeration in a bath and greatly impair the performance of the resultant composite coating. To overcome this issue, our research group developed TiO₂

sol-enhanced electrodeposition to reach nanoparticles' excellent dispersion and chemical stability in electrolytes. The TiO₂-incorporated composite coatings show improvements in mechanical and corrosion performance. When adding the TiO₂ sol to the plating bath, TiO₂ nanoparticles could be generated and directly co-deposited on the substrate's surface with metal ions, effectively preventing nanoparticle agglomeration. The excellent dispersion of nanoparticles gives rise to a uniform, compact surface structure and an excellent coating performance.

Diverse Co–Ni–TiO₂ films with superior performance were electrodeposited using TiO₂ sol at various contents. Microstructure, phase composition, mechanical properties, and corrosion performance of Co–Ni–TiO₂ films have been examined at diverse contents of TiO₂ sols. The Co–Ni film's mechanical properties and corrosion resistance can be greatly improved if TiO₂ sol is present in a suitable amount, enhancing its utility in industrial use.

2. Experimental

2.1. TiO₂ Sol Preparation

All reagents were purchased from Beijing Chemical Ltd. (Beijing, China) and used at analytical grade without further purification. The method of preparing TiO₂ sol comprises the following three steps: (1) preparation of solution A: adding 5.64 mL of C₄H₁₁NO₂ (diethanolamine) to 70 mL of C₂H₅OH (ethanol) with adequate stirring, followed by slowly dripping 19.74 mL of C₁₆H₃₆O₄Ti (tetrabutyl titanate) into the as-prepared solution under a stirring speed of 300 rpm; (2) preparation of solution B: mix 9 mL of C₂H₅OH and 0.9 mL of distilled water; and (3) solution B was added dropwise into solution A, after which the bath was stirred 500 rpm for 30 min to produce TiO₂ sol.

This study mixed 10 mL of TiO₂ sol with 100 mL of di-ionized (DI) water under ultrasonic agitating, with the purpose of producing and determining the in situ created TiO₂ nanoparticles. After the solution was dropped on a copper mesh and dried, the fresh nanoparticle could be observed.

2.2. Electrodeposition of Co–Ni–TiO₂ Films

This experiment produced Co–Ni–TiO₂ films in the electrodeposition process and used the brass sheet as a cathode and the high-purity cobalt board as an anode. To generate TiO₂ nanoparticles in situ, TiO₂ sol was slowly added to the Co–Ni electrolyte at magnetic stirring prior to electrodeposition. It should be noted that the attached organic chains in the freshly formed nanoparticles further avoid possible agglomerations.

The electrolytes used in the experiment consisted of 70 g/L NiSO₄ (nickel sulfate), 50 g/L NiCl (nickel chloride), 60 g/L CoSO₄ (cobalt sulfate), 50 g/L H₃BO₃ (boric acid), 0.015 g/L C₁₂H₂₅SO₄Na (sodium dodecyl sulfate), and 0.15 g/L C₇H₅NO₃S (saccharin). The electrodeposition temperature was 50 °C and the stirring rate was 300 rpm. Composite electrodeposition was performed at the current density of 25 mA/cm² for 40 min with various concentrations of TiO₂ sol.

2.3. Sample Characterization

This work used a transmitting electron microscope to characterize the newly generated nanoparticles (HRTEM, FEI Talos F200X G2, Thermo Fisher Scientific, Santa Clara, CA, USA). The samples' surface morphology, cross-sectional morphology, and wear track morphology were observed using a Gemini SEM 300 electron microscope with an embedded EDS detector manufactured by Zeiss Company, Jena, Germany. A 90-plus zeta potential analyzer (Malvern Zetasizer Nano ZS, Malvern, UK) was employed to investigate the zeta potential of a composite plating solution in order to determine the dispersibility and stability of TiO₂ nanoparticles. The phase constituents of the Co–Ni–TiO₂ films were analyzed by Cu–K α radiation (XRD, Bruker, Saarbrücken, Germany).

The Co–Ni–TiO₂ film's hardness was determined by a Vickers microhardness analyzer using 50 g for 15 s. The wear performance of the Co–Ni–TiO₂ films was determined

using a micro-tribometer (UMT-2, CETR, New York, NY, USA). In the wear tests, steel balls 4 mm in diameter and a load of 5 N were used under a wear speed of 10 mm/s.

With the aid of an electrochemical workstation (CS2350, Corrtest, Wuhan, China), the Co–Ni–TiO₂ films' electrochemical performance was evaluated. The platinum plate with dimensions of 10 mm × 10 mm × 0.3 mm served as the counter electrode, while a saturated KCl electrode served as the reference electrode. When the open circuit potential had been stabilized, the samples were tested at room temperature at a scanning speed of 1 mV/s using 3.5 wt.% NaCl solution.

3. Results and Discussion

3.1. Characterization of TiO₂ Sol

Figure 1 presents the TEM images recorded on the generated TiO₂ nanoparticles made by adding sol into DI water. Figure 1a shows that the TiO₂ nanoparticles are agglomerated in the drying process, but some individual nanoparticles can still be identified. The TiO₂ nanoparticles agglomerate into various-sized spheres under the TEM observations shown in Figure 1b. Some TiO₂ nanoparticle agglomerates can be found, and the separated TiO₂ nanoparticles show a particle diameter of no more than 100 nm.

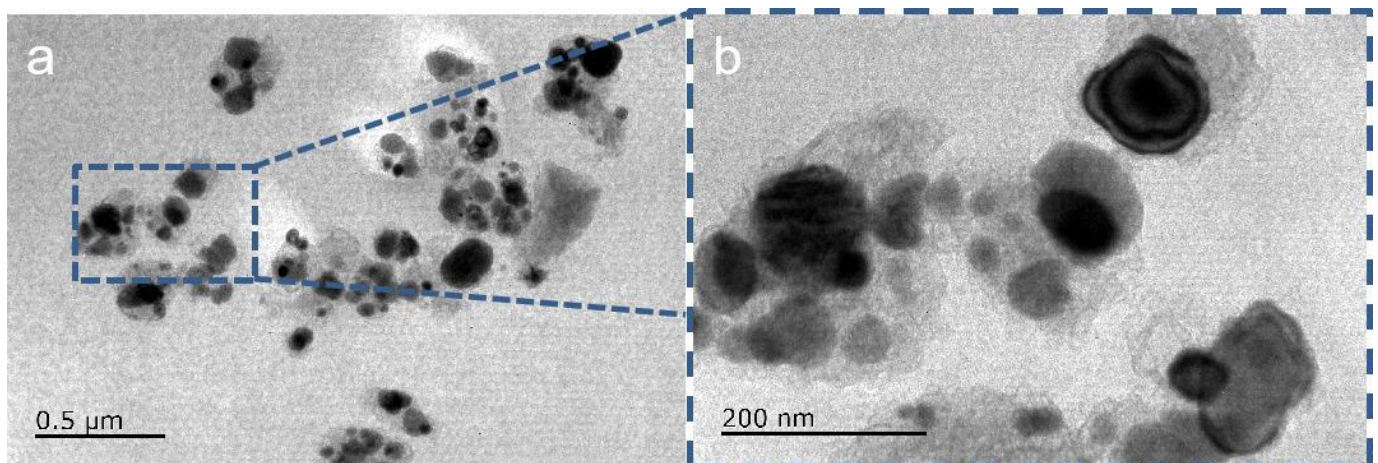


Figure 1. TEM images were taken on the generated TiO₂ nanoparticles made by adding sol into DI water. (a) TEM image, (b) Enlarged image for nanoparticles.

To confirm the existence of the produced nanoparticles, the individual TiO₂ nanoparticle was observed and analyzed. The particle size that was observed is approximately 80 nm, as illustrated in Figure 2a, with an interplanar space of 0.354 nm. Moreover, the electron diffraction pattern reveals the presence of anatase-type nanoparticles, as depicted in Figure 2b,c.

The particle size distribution of TiO₂ nanoparticles generated in DI water is further determined in Figure 3. The recorded size distribution map indicates that the average size of TiO₂ nanoparticles ranges from ~20 to ~100 nm in distilled water. This is consistent with the findings from the above TEM microscopic morphology observation. We note that the zeta potential measured a slightly smaller size distribution than the TEM images, which may be the result of aggregation occurring in the drying process prior to the TEM observation.

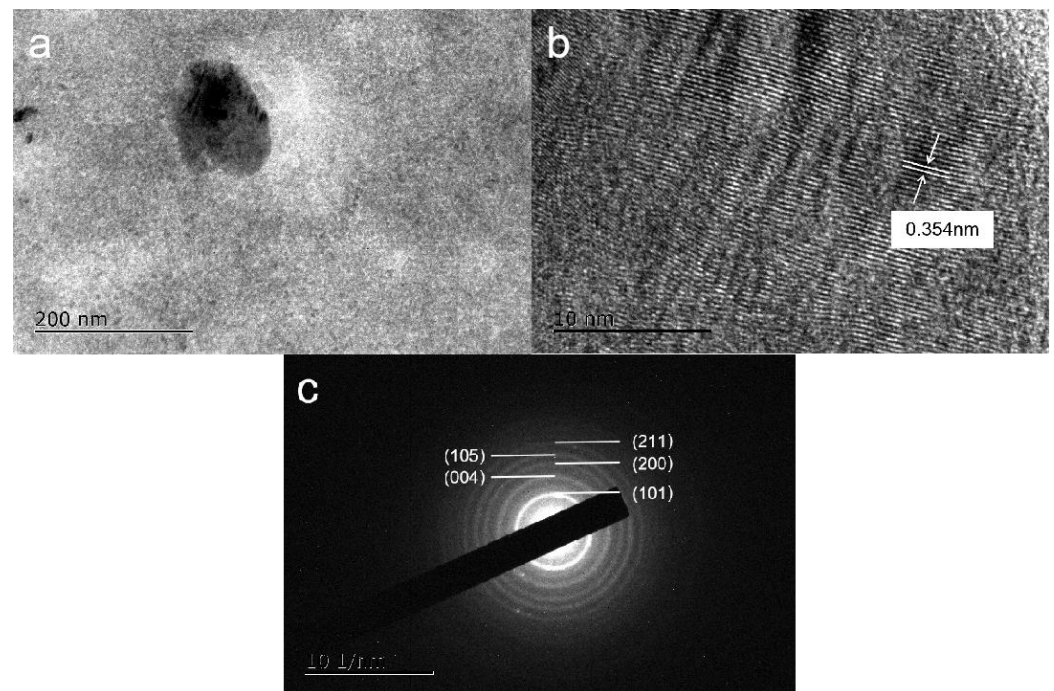


Figure 2. The microstructure of a single TiO_2 nanoparticle. (a) TEM image, (b) HR-TEM micrograph, (c) electron diffraction pattern.

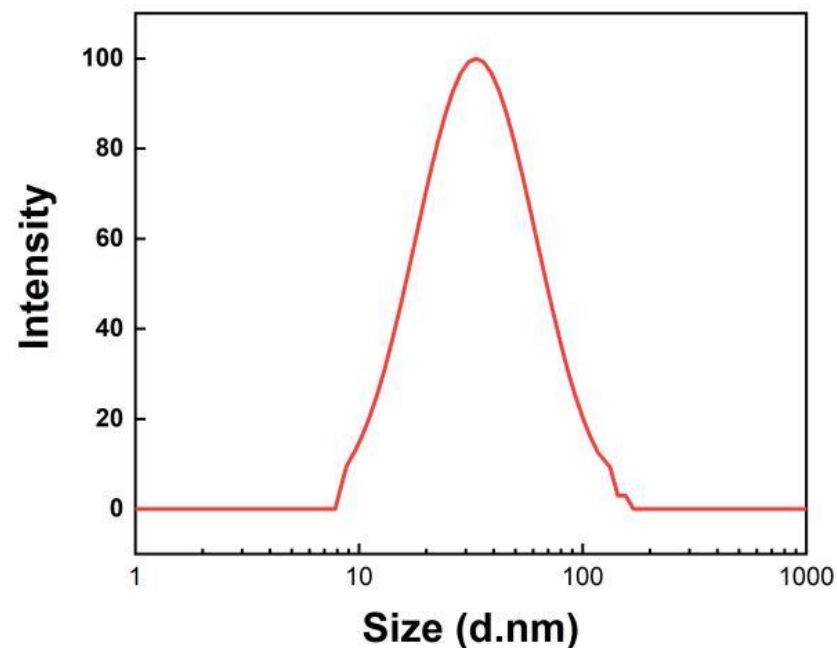


Figure 3. Size distribution of TiO_2 nanoparticles generated by adding sol into DI water.

3.2. Structural Characterizations of Co-Ni-TiO₂ Films

Figure 4 depicts the microscopic surface morphologies of Co-Ni-TiO₂ films produced by varied TiO₂ concentrations. The surface of the Co-Ni-TiO₂ films is refined and has the most significant surface uniformity and coverage at 12.5 mL/L TiO₂ sol. However, Co-Ni-50 mL/L TiO₂ film's grains are coarsened. In general, highly dispersed TiO₂ nanoparticles provide more nucleation sites, promoting nucleation processes and refining surface crystals. However, the excessive TiO₂ nanoparticles can result in agglomeration and coating coarsening under 50 mL/L TiO₂ sol.

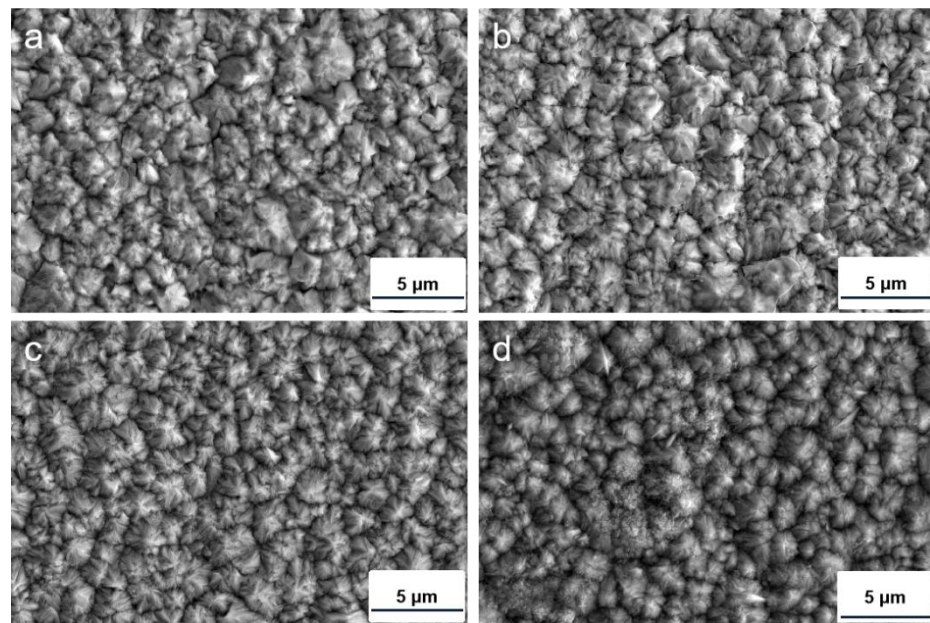


Figure 4. Surface morphology of Co–Ni–TiO₂ films prepared with different content of TiO₂ sol: (a) 0 mL/L; (b) 5 mL/L; (c) 12.5 mL/L; (d) 50 mL/L.

X-ray diffractograms of Co–Ni–TiO₂ films with diverse TiO₂ sol content are shown in Figure 5. The (220) diffraction peak is distinct in the Co–Ni–TiO₂ diffractograms. In addition, the location of the textured peak is a bit different from the standard peak due to the insertion of Ni atoms into the Co atom's structure, which is consistent with some previous papers [4,9,26]. Because there is very little content of TiO₂ nanoparticles incorporated in the Co–Ni film, no TiO₂ diffraction peak was observed in the profiles.

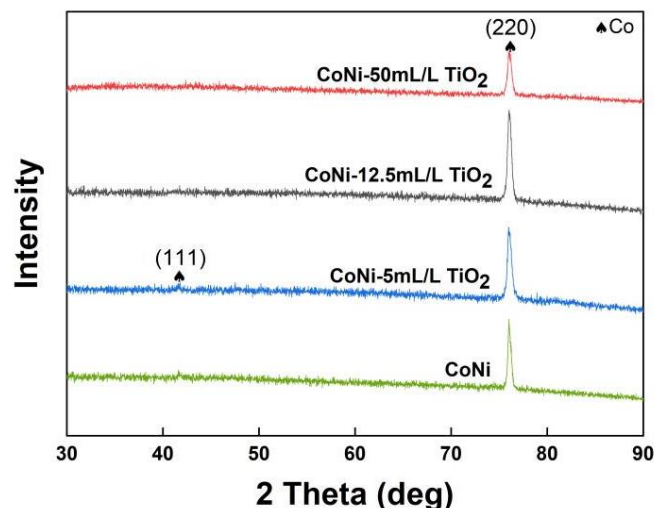


Figure 5. X-ray diffractograms recorded on the prepared Co–Ni–TiO₂ films.

Figure 6 shows the cross-sectional morphology of the composite films prepared. The coated composite film tightly adheres to the substrate with no defects, such as peeling and holes, indicating a good coating quality for all samples. In addition, no TiO₂ agglomeration regions are identified on the cross-sectional morphologies. However, the film thickness decreases at 50 mL/L sol addition. When excessive TiO₂ sol was added to the electrolyte, the electrodeposition process could be hindered and more charged current would be consumed in the side reaction of hydrogen evolution, thereby decreasing the film thickness.

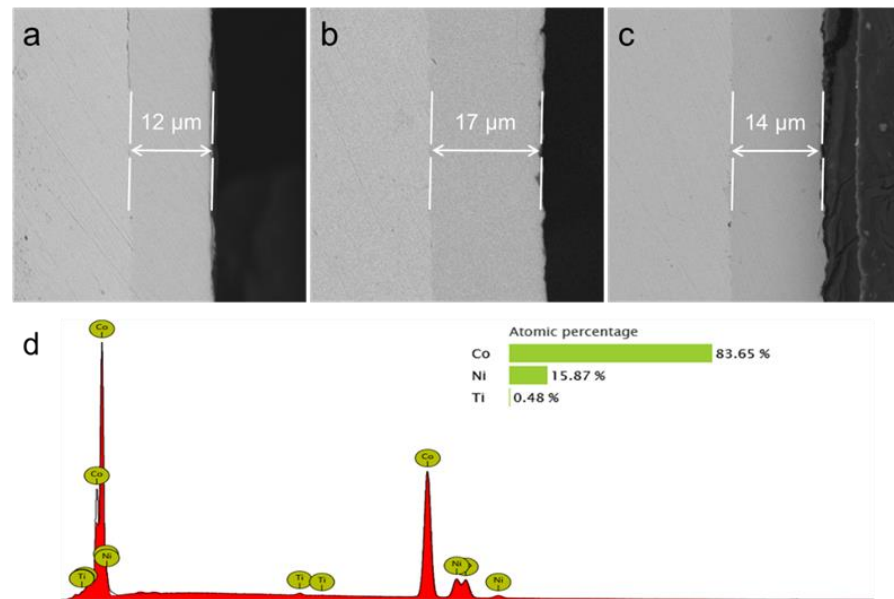


Figure 6. Cross-section of Co–Ni–TiO₂ films prepared with different content of TiO₂ sol: (a) 0 mL/L; (b) 12.5 mL/L; (c) 50 mL/L, and (d) the EDS results of the Co–Ni–12.5 mL/L TiO₂ sample.

The elemental composition obtained by EDS detection of the Co–Ni–12.5 mL/L TiO₂ sample is depicted in Figure 6d. The Co element, which has an atomic ratio of 83.78%, and the Ni element, which has an atomic ratio of 15.87%, are the main components in the prepared film according to the EDS results. There is a limited amount of Ti in the film, resulting from the incorporated TiO₂.

3.3. Mechanical Properties of Co–Ni–TiO₂ Films

The microhardness of Co–Ni–TiO₂ films at diverse TiO₂ sol content has been shown in Figure 7. The microhardness of the Co–Ni film is ~228 HV. Co–Ni–12.5 mL/L TiO₂ film possesses the highest microhardness of 323 HV, which is 41% higher than the Co–Ni film's hardness. However, adding 50 mL/L TiO₂ sol reduces the microhardness of the film to approximately 190 HV. Under an appropriate content of TiO₂ incorporation, the highly dispersed TiO₂ nanoparticles are spread in the grain boundary region, which hinders grain development and enhances fine-grain strengthening. Additionally, the highly dispersed TiO₂ nanoparticles perform the second-phase reinforcing effect that further promotes film hardness. In contrast, under an extremely high TiO₂ sol concentration, the excessive TiO₂ nanoparticle clusters cause agglomerations and reduce the films' mechanical properties.

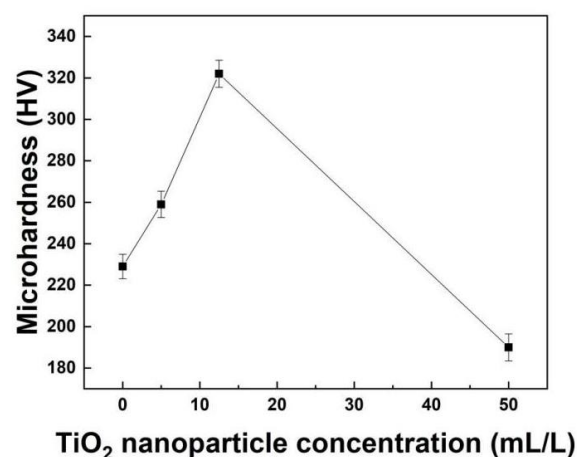


Figure 7. Microhardness tested on Co–Ni–TiO₂ films with diverse TiO₂ sol content.

Figure 8 illustrates the average friction coefficient of the Co–Ni–TiO₂ films. A Co–Ni film with no TiO₂ sol has a coefficient of 0.68, whereas a Co–Ni–12.5 mL/L TiO₂ film shows a friction coefficient of 0.42. In contrast, when the content of TiO₂ sol is 50 mL/L, the coefficient of friction increases to 0.78. The film's friction resistance will be increased using the proper TiO₂ sol (12.5 mL/L) content of the electrodeposition solution.

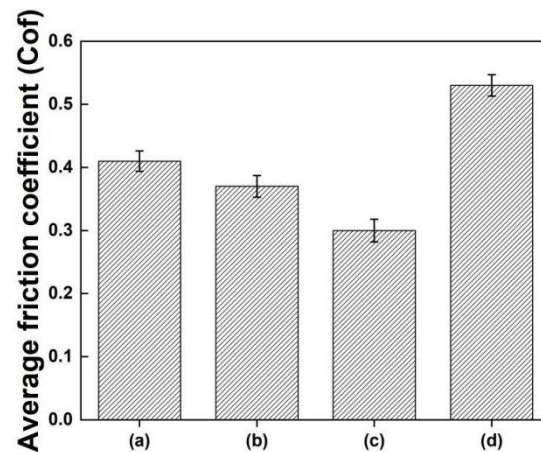


Figure 8. The friction coefficient of Co–Ni–TiO₂ films prepared with diverse content of TiO₂ sol: (a) 0 mL/L; (b) 5 mL/L; (c) 12.5 mL/L; (d) 50 mL/L.

Figure 9 illustrates the after-wear sample morphologies of Co–Ni films, Co–Ni–5 mL/L TiO₂, Co–Ni–12.5 mL/L TiO₂, and Co–Ni–50 mL/L TiO₂ films, respectively. Under the rising concentration of TiO₂ sol, the film's wear track width reduces first and then rises. A suitable content of TiO₂ sol added to the electrolytes decreases the wear track width of Co–Ni–12.5 mL/L TiO₂ to 281 μm, while the wear track width of Co–Ni–50 mL/L TiO₂ increases to about 417 μm under a higher sol concentration. The same trend is proposed: the wear resistance improves at a proper TiO₂ concentration, whereas it reduces by adding excessive TiO₂ sol.

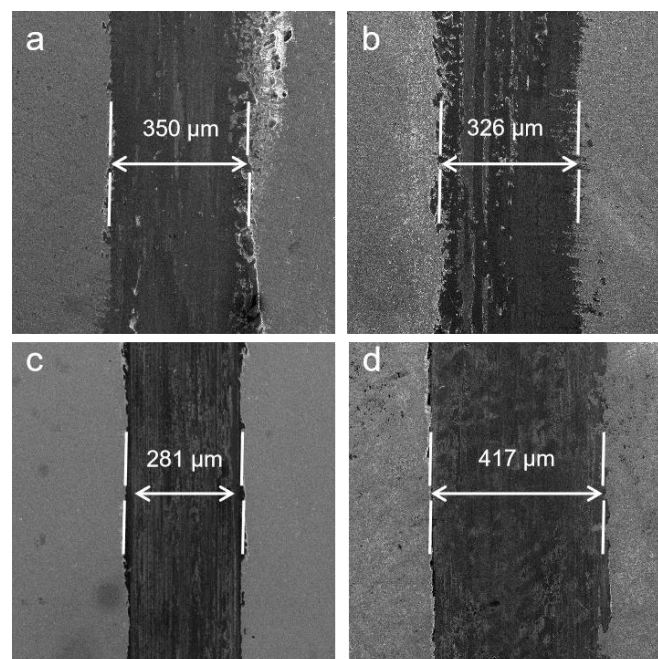


Figure 9. Wear track of Co–Ni–TiO₂ films prepared with different concentrations of TiO₂ sol: (a) 0 mL/L; (b) 5 mL/L; (c) 12.5 mL/L; (d) 50 mL/L.

3.4. Corrosion Resistance of Co–Ni–TiO₂ Films

The corrosion performance of the produced Co–Ni–TiO₂ films was investigated by measuring potentiodynamic polarization, as depicted in Figure 10. The greater the corrosion potential (E_{corr}) value of the material and the smaller the corrosion current density, the better the corrosion resistance of the film material. When the concentration of the TiO₂ sol rises, the corrosion potential of the film gradually increases. Under a 12.5 mL/L TiO₂ sol addition, the corrosion potential is the largest, showing that the film has the most excellent corrosion resistance. It is evident that the film has a worsened corrosion resistance when TiO₂ sol content reaches 50 mL/L.

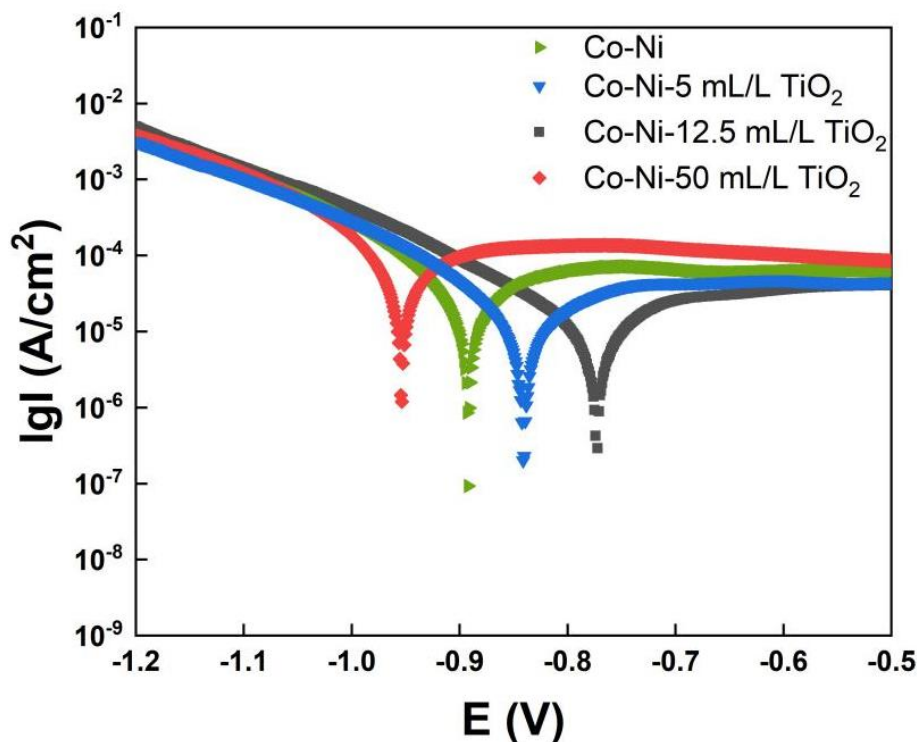


Figure 10. Potentiodynamic polarization curves of different Co–Ni–TiO₂ films.

Table 1 below shows the electrochemical parameters by fitting the polarization curves. The corrosion speed of the Co–Ni film is 0.074 mm/a, and the corrosion speed of the Co–Ni–12.5 mL/L TiO₂ film is only 0.036 mm/a. According to the findings, the corrosion resistance of the Co–Ni film is improved when the film has 12.5 mL/L TiO₂ sol. The corrosion rate for the Co–Ni–50 mL/L TiO₂ film is 0.171 mm/a, indicating that the film’s corrosion resistance significantly decreases. Adding appropriate content of TiO₂ sol can form a denser film surface with refined crystals, as suggested above, which explains the enhanced corrosion performance. Nevertheless, an excessive concentration of TiO₂ sol will cause TiO₂ nanoparticles to agglomerate in the coating, impairing the coating’s uniformity and decreasing the corrosion resistance.

Table 1. Potential polarization data of Co–Ni–TiO₂ films.

Sample	E_{corr} (V)	I_{corr} ($\mu\text{A}/\text{cm}^2$)	Corrosion Rate (mm/a)
Co–Ni	–0.88	6.28	0.074
Co–Ni–5 mL/L TiO ₂	–0.84	3.69	0.054
Co–Ni–12.5 mL/L TiO ₂	–0.76	3.09	0.036
Co–Ni–50 mL/L TiO ₂	–0.99	14.6	0.171

4. Conclusions

This study utilized chemical synthesis to create TiO₂ sols with high dispersion and chemical stability. Mechanical and corrosion-resistant Co–Ni–TiO₂ films were prepared by adding a suitable amount of TiO₂ sol (12.5 mL/L) to the electrolytes during electrodeposition. The addition of TiO₂ sol controls the nucleation process and the properties of the composite films by generating TiO₂ nanoparticles in situ in the electrodeposition process. By producing TiO₂ nanoparticles in situ in electrolytes with sizes below 100 nm, nanoparticle agglomeration is largely avoided. The mechanical property testing results reveal that the Co–Ni–12.5 mL/L TiO₂ film has the highest hardness of 323 HV, an increase of 41% over the undoped samples. Electrochemical tests demonstrate a 51% reduction in the corrosion rate for the Co–Ni–12.5 mL/L TiO₂ film compared to the undoped Co–Ni film sample. Increased nucleation sites can result from the appropriate amount of TiO₂ sol, enhancing coating quality through fine-grain and dispersion-strengthening effects. Nevertheless, coarse grains and pores will result from the agglomeration of excessive TiO₂ nanoparticles under high TiO₂ sol concentration, which will have a detrimental impact on the film's performance.

Author Contributions: Conceptualization, Y.W. and Z.H.; methodology, Z.M. and J.C.; validation, Z.H. and Z.M.; formal analysis, Z.H.; investigation, Z.M.; writing—original draft preparation, Y.W.; writing—review and editing, Z.H.; visualization, S.Z.; supervision, J.C. and Z.H.; funding acquisition, Z.H. All authors have read and agreed to the published version of the manuscript.

Funding: This work was supported by the Natural Science Foundation of Jiangsu Province by grant BK20201008.

Institutional Review Board Statement: Not applicable.

Informed Consent Statement: Not applicable.

Data Availability Statement: Not applicable.

Conflicts of Interest: The authors declare no conflict of interest.

References

1. Bouziti, F.Z.; Nemamcha, A.; Moumeni, H.; Rehspringer, J.L. Morphology and Rietveld analysis of nanostructured Co-Ni electrodeposited thin films obtained at different current densities. *Surf. Coat. Technol.* **2017**, *315*, 172–180. [[CrossRef](#)]
2. Olvera, S.; Arce Estrada, E.M.; Sanchez-Marcos, J.; Palomares, F.J.; Vazquez, L.; Herrasti, P. Effect of the low magnetic field on the electrodeposition of Co_xNi_{100-x} alloys. *Mater. Charact.* **2015**, *105*, 136–143. [[CrossRef](#)]
3. Li, D.; Levesque, A.; Franczak, A.; Wang, Q.; He, J.; Chopart, J.P. Evolution of morphology in electrodeposited nanocrystalline Co-Ni films by in-situ high magnetic field application. *Talanta* **2013**, *110*, 66–70. [[CrossRef](#)] [[PubMed](#)]
4. Karpuz, A.; Kockar, H.; Alper, M. Electrodeposited Co–Ni Films: Electrolyte pH—Property Relationships. *J. Supercond. Nov. Magn.* **2012**, *26*, 651–655. [[CrossRef](#)]
5. Yu, M.M.; Li, H.Y.; Wang, Y. Study on Present Situation and New Trends of the Electrodeposition of Nickel-Cobalt Alloy. *Adv. Mater. Res.* **2012**, *535–537*, 973–976. [[CrossRef](#)]
6. Sun, L.F.; Mao, J.M.; Pan, Z.W.; Chang, B.H.; Zhou, W.Y.; Wang, G.; Qian, L.X.; Xie, S.S. Growth of straight nanotubes with a cobalt–nickel catalyst by chemical vapor deposition. *Appl. Phys. Lett.* **1999**, *74*, 644–646. [[CrossRef](#)]
7. Li, Y.; Xie, Y.; Huang, L.; Liu, X.; Zheng, X. Effect of physical vapor deposited Al₂O₃ film on TGO growth in YSZ/CoNiCrAlY coatings. *Ceram. Int.* **2012**, *38*, 5113–5121. [[CrossRef](#)]
8. Cuglietta, M.; Kuhn, J.; Kesler, O. A Novel Hybrid Axial-Radial Atmospheric Plasma Spraying Technique for the Fabrication of Solid Oxide Fuel Cell Anodes Containing Cu, Co, Ni, and Samaria-Doped Ceria. *J. Therm. Spray Technol.* **2013**, *22*, 609–621. [[CrossRef](#)]
9. Liu, C.; Su, F.; Liang, J. Nanocrystalline Co-Ni alloy coating produced with supercritical carbon dioxide assisted electrodeposition with excellent wear and corrosion resistance. *Surf. Coat. Technol.* **2016**, *292*, 37–43. [[CrossRef](#)]
10. Hu, H.; Tan, M.; Liu, L. Anomalous codeposition mechanism of Co-Ni alloy nanowires. *J. Alloys Compd.* **2017**, *715*, 384–389. [[CrossRef](#)]
11. Barzegar, M.; Allahkaram, S.R.; Naderi, R.; Ghavidel, N. Effect of phosphorous content and heat treatment on the structure, hardness and wear behavior of Co-P coatings. *Wear* **2019**, *422–423*, 35–43. [[CrossRef](#)]
12. Tebbakh, S.; Messaoudi, Y.; Azizi, A.; Fenineche, N.; Schmerber, G.; Dinia, A. The influence of saccharin on the electrodeposition and properties of Co–Ni alloy thin films. *Trans. IMF* **2015**, *93*, 196–204. [[CrossRef](#)]

13. Altamirano-Garcia, L.; Vazquez-Arenas, J.; Pritzker, M.; Luna-Sánchez, R.; Cabrera-Sierra, R. Effects of saccharin and anions (SO_4^{2-} , Cl^-) on the electrodeposition of Co–Ni alloys. *J. Solid State Electrochem.* **2014**, *19*, 423–433. [[CrossRef](#)]
14. Vazquez-Arenas, J.; Treeratanaphitak, T.; Pritzker, M. Formation of Co–Ni alloy coatings under direct current, pulse current and pulse-reverse plating conditions. *Electrochim. Acta* **2012**, *62*, 63–72. [[CrossRef](#)]
15. Wang, S. Influence of 2-butyne-1, 4-diol on the structure and performance of the Co–Ni alloy plated by electrodeposition. *Acta Metall. Sin.* **2008**, *21*, 50–56. [[CrossRef](#)]
16. Bu, A.; Zhang, Y.; Zhang, Y.; Chen, W.; Cheng, H.; Wang, L.; Wang, Y. A Novel Electrolytic Plasma Spraying Preparation SiO_2/SiC Coating on Carbon Fiber Fabric. *Coatings* **2018**, *8*, 344. [[CrossRef](#)]
17. Xiong, C.; Xiao, J.; Zhao, Y.; Wang, Y.; Tay, S.L.; Xu, W. Properties of Ni– ZrO_2 nanocomposite coatings by electroplating. *Int. J. Mod. Phys. B* **2019**, *33*, 1940024. [[CrossRef](#)]
18. Zhang, W.; Du, S.; Li, B.; Mei, T.; Miao, Y.; Chu, H.; Wang, J. Synthesis and characterization of TiN nanoparticle reinforced binary Ni–Co alloy coatings. *J. Alloys Compd.* **2021**, *865*, 158722. [[CrossRef](#)]
19. Elkhoshkhany, N.; Hafnway, A.; Khaled, A. Electrodeposition and corrosion behavior of nano-structured Ni–WC and Ni–Co–WC composite coating. *J. Alloys Compd.* **2017**, *695*, 1505–1514. [[CrossRef](#)]
20. Wang, Y.; Hu, B.; Tay, S.L.; Hou, F.; Gao, W.; Xiong, C. The microstructure and properties of sol-enhanced Sn– TiO_2 nanocomposite coatings. *Int. J. Mod. Phys. B* **2017**, *31*, 1744025. [[CrossRef](#)]
21. He, Z.; Cao, D.; Wang, Y.; Yin, L.; Hayat, M.D.; Singh, H. Preparation of Co–P– TiO_2 nanocomposite coatings via a pulsed electrodeposition process. *Surf. Eng.* **2019**, *36*, 975–981. [[CrossRef](#)]
22. Zhang, W.; Cao, D.; Qiao, Y.; He, Z.; Wang, Y.; Li, X.; Gao, W. Microstructure and Properties of Duplex Ni–P– $\text{TiO}_2/\text{Ni–P}$ Nanocomposite Coatings. *Mater. Res.* **2019**, *22* (Suppl. 2), e20180478. [[CrossRef](#)]
23. Liu, Y.; Li, L.; Lu, G.-L.; Han, Z.-W.; Liu, J.-D.; Yu, S.-R. Fractal characteristics and wettability of Nano- $\text{Al}_2\text{O}_3/\text{Ni–Co}$ composite coating prepared by electrodeposition. *Trans. Nonferrous Met. Soc. China* **2011**, *21*, s380–s383. [[CrossRef](#)]
24. Rasooli, A.; Safavi, M.S.; Kasbkar Hokmabad, M. Cr_2O_3 nanoparticles: A promising candidate to improve the mechanical properties and corrosion resistance of Ni–Co alloy coatings. *Ceram. Int.* **2018**, *44*, 6466–6473. [[CrossRef](#)]
25. Bakhit, B.; Akbari, A.; Nasirpouri, F.; Hosseini, M.G. Corrosion resistance of Ni–Co alloy and Ni–Co/ SiC nanocomposite coatings electrodeposited by sediment codeposition technique. *Appl. Surf. Sci.* **2014**, *307*, 351–359. [[CrossRef](#)]
26. Gómez, E.; Pané, S.; Alcobe, X.; Vallés, E. Influence of a cationic surfactant in the properties of cobalt–nickel electrodeposits. *Electrochim. Acta* **2006**, *51*, 5703–5709. [[CrossRef](#)]

Disclaimer/Publisher’s Note: The statements, opinions and data contained in all publications are solely those of the individual author(s) and contributor(s) and not of MDPI and/or the editor(s). MDPI and/or the editor(s) disclaim responsibility for any injury to people or property resulting from any ideas, methods, instructions or products referred to in the content.